Tuning short-range attractions in protein solutions: from attractive glasses to equilibrium clusters

2005 J. Phys.: Condens. Matter 17 S2805

(http://iopscience.iop.org/0953-8984/17/31/005)

INSTITUTE OF PHYSICS PUBLISHING JOURNAL OF PHYSICS: CONDENSED MATTER

J. Phys.: Condens. Matter **17** (2005) S2805–S2816 doi:10.1088/0953-8984/17/31/005

Tuning short-range attractions in protein solutions: from attractive glasses to equilibrium clusters

Anna Stradner[1], **George M Thurston**[2] **and Peter Schurtenberger**[1,3]

[1] Department of Physics, University of Fribourg, Chemin du Musée 3, CH-1700 Fribourg, Switzerland
[2] Department of Physics, Rochester Institute of Technology, 85 Lomb Memorial Drive, Rochester, NY 14623-5603, USA

E-mail: peter.schurtenberger@unifr.ch

Received 23 December 2004, in final form 10 February 2005
Published 22 July 2005
Online at stacks.iop.org/JPhysCM/17/S2805

Abstract

We report small-angle scattering experiments with two different types of model proteins, lysozyme and the eye lens protein γB-crystallin. We discuss the results in the context of recent suggestions that globular proteins possess a short-ranged attractive potential, and that simple models from colloid science could help to rationalize the best route for obtaining protein crystals and to interpret their complex phase diagrams. The short-range attraction leads to an extremely interesting phase behaviour with a liquid–gas coexistence curve that is metastable with respect to the liquid–solid (crystal) boundary and the occurrence of an attractive glass. We demonstrate that for γB-crystallin, the scattering data are indeed in good agreement with predictions for an interaction potential consisting of short-ranged attraction and hard sphere repulsion, and we also provide evidence of a dynamically arrested glass or gel phase at high concentrations. We also report on a systematic study of the effect of a weak screened Coulomb repulsion in highly concentrated lysozyme solutions. We demonstrate that combining short-range attraction and long-range repulsion results in the formation of small equilibrium clusters, and we discuss the concentration and temperature dependence of the cluster size in view of its analogy to micelle formation.

1. Introduction

Colloidal suspensions have frequently been used as ideal model systems for investigating various aspects of phase equilibria such as the formation, extent and static and dynamic properties of crystal and glass phases. They offer access to scales of length and time that are well suited for experimentalists and allow for a variation of the form, strength and

[3] Author to whom any correspondence should be addressed.

range of the interaction potential almost at will. With the equilibrium behaviour of colloidal systems seemingly well understood, attention recently turned to nonequilibrium phenomena. In particular the influence of a short-ranged attractive potential has been intensively investigated theoretically and experimentally, and this concerted effort of the scientific community has led to fascinating findings which include metastable liquid–liquid phase separation and dynamically arrested states such as attractive and repulsive glasses as well as transient gels [1–7].

In these attempts to develop and use suitable model systems that interact via a (tunable) short-range attractive potential a number of groups have relied on colloids interacting via a so-called depletion potential, where the range and strength of the attractive interactions can be tuned by the addition of a non-adsorbing polymer [4, 5, 8–11]. Such systems have indeed recently allowed verification of the most important theoretical predictions for short-range attractions. These include the possibility for coexistence of two crystal or glass structures at high densities and a re-entrant glass–fluid–glass transition [4, 5, 8, 10]. However, at high densities and the correspondingly high polymer concentrations the situation becomes difficult, and the commonly used simple model potentials can in principle not be applied. Moreover, while these systems allow for almost complete density and index of refraction matching due to the use of appropriate (organic) solvent mixtures, this has also raised questions as to the possible influence of residual charges on the existence of a cluster phase prior to gel or glass formation [12–15].

Possible alternatives to circumvent these problems are globular proteins. Different globular proteins have been shown to exhibit the major hallmarks of colloids interacting via a short-range attractive potential. At high ionic strength, where the salt screens the electrostatic repulsions that are also present, the short-range attractions increasingly dominate with decreasing temperature. This leads to a liquid–liquid phase separation and the related critical phenomena, which are metastable with respect to the liquid–crystal coexistence line [16–20]. A physiologically important example is that of the γ-crystallins, globular proteins of molecular mass near 21 kDa [18, 20–31]. The γ-crystallins are a component of the eye lens proteins of mammals, where the opacity of the lens due to critical scattering and phase separation is one reason for cataract formation. The γ-crystallins are one of the most studied classes of eye lens proteins.

Another prime candidate as a model for attractive colloids is the highly stable and extensively investigated lysozyme [18, 19, 32]. Lysozyme is a globular protein with a radius of about 1.7 nm and unlike γ-crystallins has a high net charge near neutral pH. At high ionic strength, where the salt screens the electrostatic repulsions between the charged proteins, it has been shown to behave like colloidal particles with a short-range attractive potential. It not only exhibits a metastable liquid–liquid phase separation, but shows evidence for a glass line or gel line at relatively low volume fractions, in agreement with predictions from mode-coupling theory for colloids with short-range attraction [16].

Such a scenario with a metastable liquid–liquid coexistence curve and a gel line obviously affects the ability to form high-quality crystals required for protein crystallography [17]. Moreover, the issues of interparticle interaction, aggregation, cluster and crystal formation and dynamical arrest are of central importance to a variety of topics ranging from cluster formation in various diseases [33] to the production of photonic crystals. We thus have the long-term aim of understanding the combined effects of short-ranged attraction and hard and/or soft repulsion on the phase behaviour of a wide range of colloidal suspensions.

Here we summarize an experimental study of two different model proteins, γB-crystallins and lysozyme, which have both common and contrasting properties. For γB-crystallin, we have chosen conditions of high ionic strength that fully screen electrostatic repulsions. In the present buffer γB-crystallin exhibits metastable liquid–liquid phase separation with a critical

point at $c_c = 260$ mg ml^{-1} and $T_c \approx 15\,^{\circ}$C. Due to its extreme stability, γB-crystallin is an ideal model for investigating the influence of the short-range attraction on the static and dynamic structure factor up to very high concentrations.

In the case of lysozyme, however, we have looked at concentrated solutions at relatively low ionic strength to study the effect of charges on their structure. The absence of added salt in the protein solution leads to a modified interaction potential, which now consists of a weakly screened repulsive Coulomb part in addition to the short-range attraction and hard core repulsion. We have recently been able to provide the first experimental confirmation that a combination of short-range attraction and long-range repulsion results in the formation of small equilibrium clusters [34]. This finding clearly is relevant for a range of practically important phenomena including nucleation processes during protein crystallization, protein or DNA self-assembly, and the previously observed formation of cluster and gel phases in colloidal suspensions [14, 15, 17, 32]. In the current study we now investigate the effect of variations in temperature, which allow us to carefully tune the balance between soft repulsion and short-range attraction and investigate its influence on the cluster formation.

Any attempt to use the theoretical framework for strongly interacting colloidal particles, for example, to use mode-coupling theory to evaluate particle dynamics close to dynamical arrest near a glass or gel line, requires precise knowledge of the static structure factor $S(q)$. We have thus used a combination of small-angle x-ray and neutron scattering (SAXS and SANS) to determine $S(q)$ as a function of concentration, ionic strength and temperature for both lysozyme and γB-crystallin. This provides structural information on the spatial correlations between individual proteins in concentrated solutions.

2. Materials and methods

2.1. Preparation of lens protein solutions

γB-crystallins were isolated from third-trimester prenatal to six-week-old calf lenses using size-exclusion chromatography of nuclear fractions on Sephacryl S-200, using 0.275 M Na acetate buffer, pH 4.5, followed by cation-exchange chromatography on sulfopropyl Sephadex C-50, using 0.275 M Na acetate buffer, pH 4.8, and a 0–0.3 M NaCl gradient [22, 35]. All buffers contained sodium azide (0.02%). As the solvent, 0.1 M phosphate buffer in D_2O including dithiothreitol (DTT, 20 mM) and sodium azide (0.02%) at pH = 7.1 was used. To reach concentrations of the order of 300–500 mg ml^{-1}, solutions of known proportions were concentrated by ultrafiltration using disposable centrifugal filtration units. Protein concentrations were determined by UV absorption using a specific absorption coefficient $E^{1\%}_{1\ \mathrm{cm}} = 21.8$ [24]. Using a partial specific volume of 0.71 cm^3 g^{-1} for the γB-crystallin proteins results in the corresponding protein monomer volume fractions of $0.2 \leqslant \phi \leqslant 0.36$.

2.2. Preparation of lysozyme solutions

Hen egg white lysozyme was obtained from Fluka (L7651, three times crystallized, dialysed and lyophilized) and used without further purification. About 40 mg protein was dissolved per ml of a 20 mM HEPES buffer in D_2O (99.9%, Cambridge Isotope Laboratories) for the samples used for SANS and in Milli-Q H_2O for the samples measured with SAXS at pH 7.8, where the lysozyme carries a net positive charge of about eight electronic charges [19, 36]. To avoid microbial attack the buffers contained 3 mM NaN_3. This stock solution was stirred at room temperature and passed through a 0.22 μm filter to remove any undissolved material. An Amicon ultrafiltration stirring cell with a YM-10 membrane was used to further concentrate it.

Small variations in the final pH as a function of protein concentration as well as temperature have no measurable effect on the cluster formation mechanism [34]. Lower concentrations were prepared by diluting the stock solution with buffer at pH 7.8. The final concentrations were determined by UV absorption spectroscopy at 280 nm using a specific absorption coefficient $E^{1\%}_{1\ \mathrm{cm}} = 26.4$; the highest concentrations were typically between 250 and 350 mg ml^{-1}. Using a partial specific volume of 0.74 cm^3 g^{-1} for the lysozyme proteins results in the corresponding protein monomer volume fractions of $0.185 \leqslant \phi \leqslant 0.26$.

2.3. Small-angle x-ray scattering measurements

SAXS experiments were carried out with a pinhole camera (NanoSTAR, Bruker AXS) equipped with a sealed tube (Cu Kα), a thermostatically regulated sample chamber and a two-dimensional gas detector. The q range is 0.1–2 nm^{-1}.

2.4. Small-angle neutron scattering measurements

SANS experiments were performed at the SANS I facility at the Swiss neutron source SINQ at the Paul Scherrer Institute, Switzerland. 1 and 2 mm quartz cells from Helma and a thermostated sample holder were used. Combinations of different wavelengths (8 and 12.67 Å), sample-to-detector distances (1.6–18 m) and collimation lengths (4.5–18 m) resulted in a q range of 0.02–4 nm^{-1}. The raw spectra were corrected for background from the solvent (D_2O buffer), sample cell and electronic noise by conventional procedures. Furthermore, the two-dimensional isotropic scattering spectra were corrected for detector efficiency by dividing with the incoherent scattering spectra of pure water and azimuthally averaged.

3. Results and discussion

3.1. Proteins with short-range attraction—γB-crystallin

In the first part of the article we summarize a systematic study of the influence of temperature and concentration on the scattering intensity of γB-crystallin solutions. We have used conditions for which the structural properties are dominated by the combination of short-ranged attraction and hard core repulsion between the proteins. The scattered intensity, I, versus scattering vector, q, was measured with small-angle neutron scattering (SANS) up to a concentration nearly twice that of the critical concentration, and as a function of temperature, as shown by the 'x's in figure 1(a). The critical temperature was estimated by visual observation of clouding of solutions near the critical concentration, and the cloud point curve previously measured for γB-crystallin was shifted in temperature to provide an estimate of the appropriate curve in the present buffer [22]. Figure 1 shows that $I(q)$ depends dramatically on both concentration and temperature, especially near the probable coexistence curve of γB-crystallin in the present D_2O buffer (dashed curve in figure 1(a)).

Two features of $I(q)$ vary in a particularly prominent manner. First, $I(q < 0.1\ \mathrm{nm}^{-1})$ becomes large when the critical point is approached. This occurs both when temperature is varied at fixed concentration (figure 1(c)), and when concentration is varied at fixed temperature (figure 1(b)). The high values of $I(q < 0.1\ \mathrm{nm}^{-1})$ reflect enhanced long-wavelength concentration fluctuations near criticality (cp in figure 1(a)), which have been well studied [20, 37–39]. Second, $I(1\ \mathrm{nm}^{-1} < q < 3\ \mathrm{nm}^{-1})$ shows a peak that grows with concentration, reflecting increased probability of protein–protein adjacency [37].

In fact, figures 1(b) and (d) also show that as concentration increases at 25 °C, the entire I versus q curve first increases and reaches a maximum in the vicinity of the critical

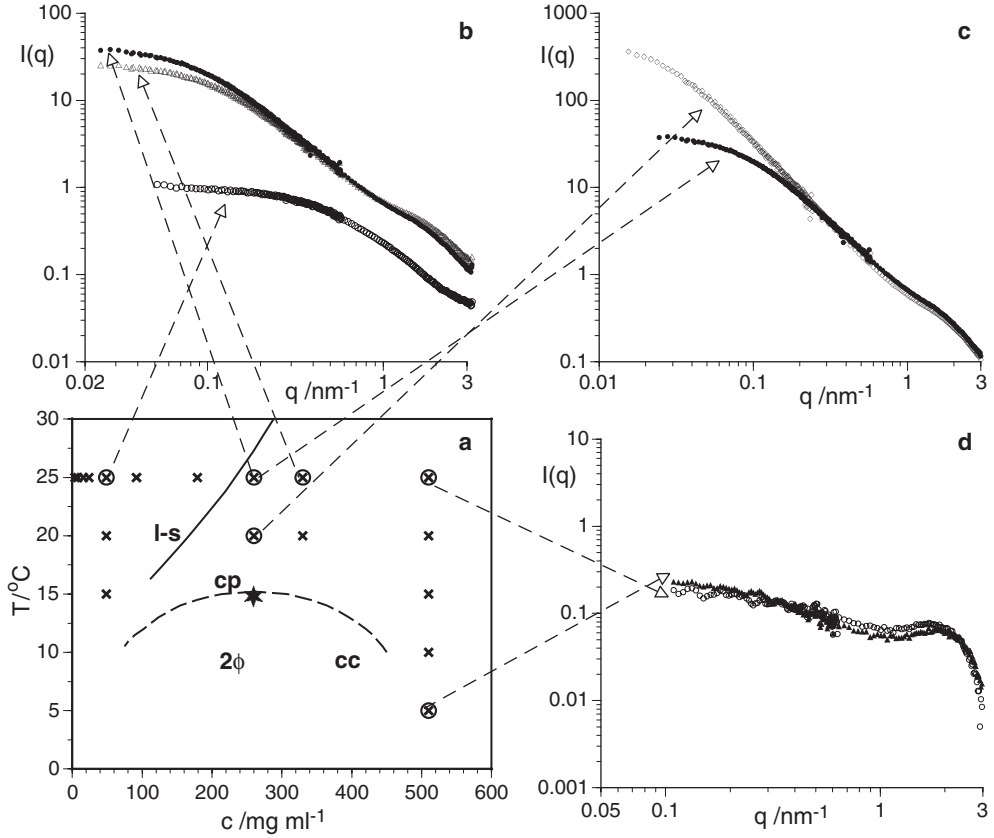

Figure 1. Neutron small-angle scattering data for γB-crystallin solutions at different locations in the phase diagram. (a) Schematic phase diagram of γB-crystallins; l–s denotes the liquid–solid phase boundary. The dashed line is the liquid–liquid coexistence curve (cc), which is metastable with respect to the liquid–solid phase boundary. The critical point cp is located at a critical temperature of $T_c \approx 15\,^{\circ}$C and a critical concentration $c_c \approx 260$ mg ml^{-1}. Crosses correspond to samples measured with SANS. (b) Scattered intensities of a 49 mg ml^{-1} (open circles), a 260 mg ml^{-1} (dots) and a 330 mg ml^{-1} (triangles) sample at 25 °C. (c) Comparison of the scattered intensities of a sample at the critical concentration at 20 °C (diamonds) and 25 °C (dots). (d) Scattering curves of a 510 mg ml^{-1} protein solution at 5 °C (triangles) and 25 °C (open circles).

concentration, before decreasing to a level at 500 mg ml^{-1} that is approximately two orders of magnitude smaller than that found above the critical concentration, at 25 °C. The striking lack of temperature dependence in the scattering from the 510 mg ml^{-1} sample suggests that this sample may be qualitatively different from the lower concentration samples. Indeed, dynamic light scattering experiments indicate that this dramatic reduction in intensity for the concentrated samples is accompanied by dynamical arrest as the sample exhibits the characteristic signs of a nonergodic glass/gel phase.

Effective structure factors $S_{\rm eff}(q)$ were obtained from the data shown in figure 1 by dividing $I(q)/c$ by the normalized intensity of a dilute sample having a concentration of 8 mg ml^{-1} and are shown in figure 2. The dependence of $S_{\rm eff}(q)$ on temperature and concentration clearly demonstrates the roles of prominent long-wavelength fluctuations near the critical point and enhanced interprotein adjacency on the observed scattering, as we now describe.

First, figure 2(a) shows that at 20 °C, the low-q $S_{\rm eff}$ increases by a factor of 50 on going from 50 mg ml^{-1}, a concentration well below the critical concentration c_c, to 260 mg ml^{-1}, very

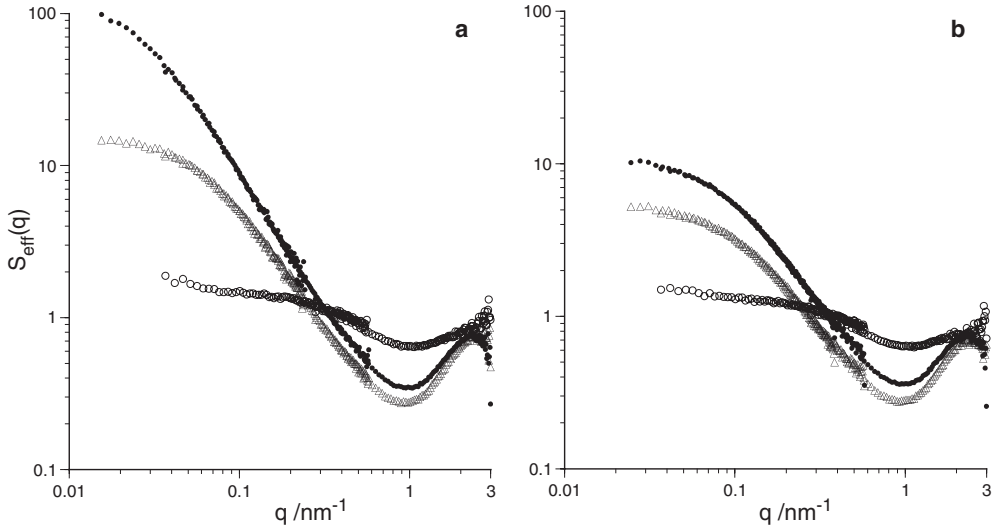

Figure 2. Effective structure factors $S_{\rm eff}(q)$ of a 49 mg ml^{-1} (open circles), a 260 mg ml^{-1} (dots) and a 330 mg ml^{-1} (triangles) γB-crystallin solution at 20 °C (a) and 25 °C (b).

near $c_{\rm c}$. The near-critical concentration fluctuations underlying this behaviour are considerably less prominent at 25 °C, which is further from the critical temperature, as shown by figure 2(b).

Second, figure 2 shows that upon increasing concentration a dip in $S_{\rm eff}(q)$ near $q = 1\,{\rm nm}^{-1}$, followed at larger q by a peak, becomes prominent. As shown previously by comparison with Monte Carlo simulations of γB-crystallin solutions [37], this feature reflects increased probability of contact between proteins at the higher concentrations. This dip and peak are sensitive primarily to concentration, and not dramatically to temperature, as can be seen by comparing the 25 °C $S_{\rm eff}(q)$ of figure 2(a) with the 20 °C $S_{\rm eff}(q)$ of figure 2(b).

Figure 3 shows results of an experiment very similar to that shown in figure 2, but with use of a different batch of γB-crystallin, in the same buffer. This preparation exhibited a lower $T_{\rm c}$, near 11 °C, so that the 25 °C data shown are further removed from the critical temperature than were the 25 °C data shown in figure 2(b). This is consistent with the observation that there is less pronounced growth in $S_{\rm eff}$ at low q upon increasing concentration, for the experiment shown in figure 3. However, the increasingly pronounced dip and peak at high q with increasing concentration in figure 3 are quite similar to the behaviour exhibited in figure 2.

Figure 3 shows that a semi-quantitative representation of the $S_{\rm eff}(q)$ data can be given by the Baxter sticky sphere liquid structure model for $S_{\rm eff}(q)$, which has been successful for modelling the light scattering efficiency of γB-crystallin solutions [39]. In figure 3(e) the data are replotted in three dimensions as a function of q and concentration, together with the Baxter model predictions. For the diameter of the spheres in the Baxter model, we have used 3.6 nm. Since the measurement temperature was approximately 15 °C above $T_{\rm c}$ for this buffer and preparation, we have used a value for the Baxter stickiness parameter, $1/\tau = 8.62$, which was found by Fine *et al* to yield a good representation of the light scattering efficiency at 15 °C above $T_{\rm c}$ for their buffer [39]. As can be seen from figures 3(a)–(e), the Baxter model shows semi-quantitative agreement with both the rise of $S_{\rm eff}(0)$ and the more pronounced dip and finite-q peak of $S_{\rm eff}(q)$, as protein concentration increases. It is important to point out that this agreement is achieved without any attempt to independently fit the individual data sets at different concentrations, but is obtained using a stickiness parameter from the literature based on independent light scattering experiments only. Moreover, the theoretical curves

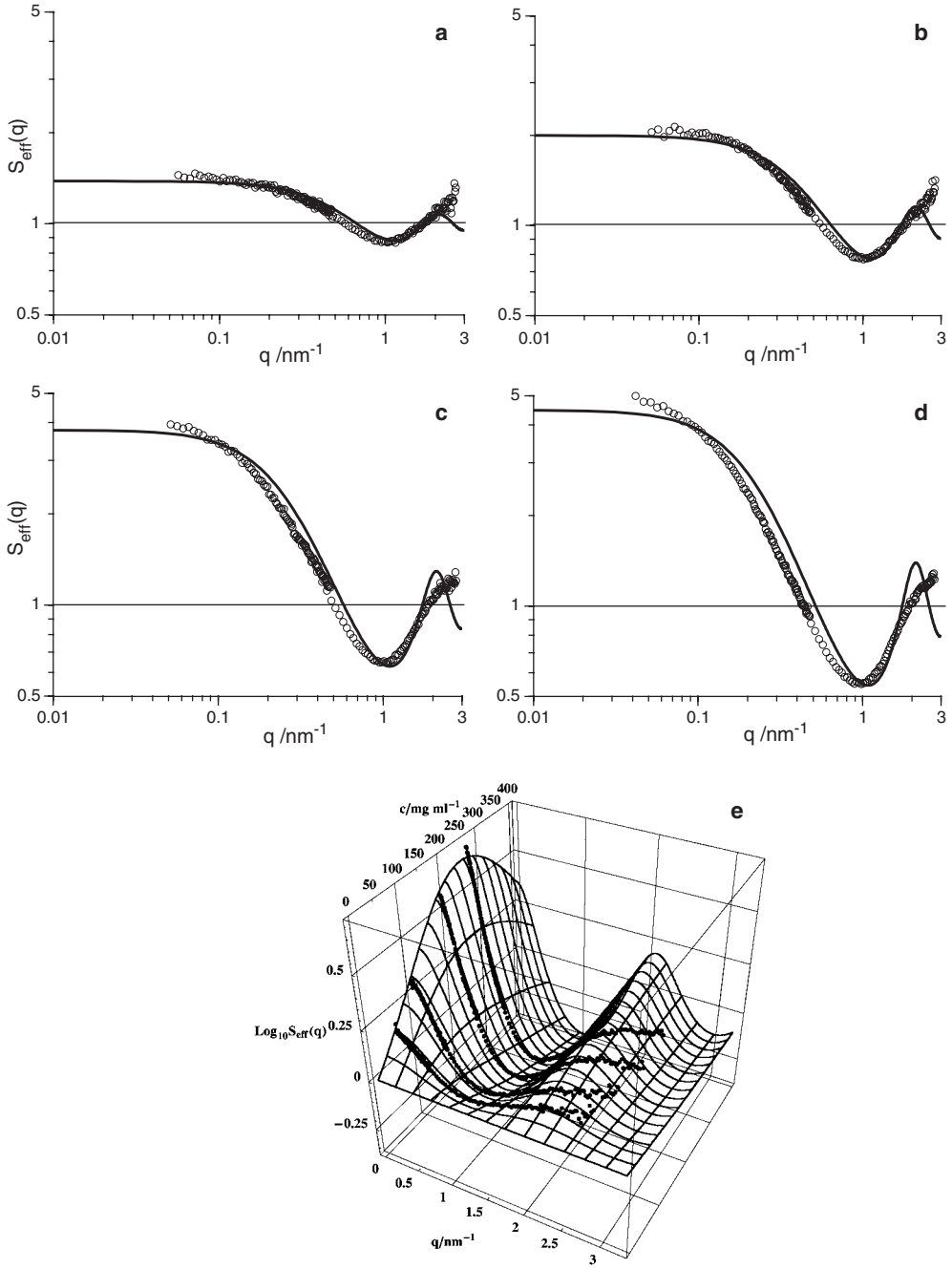

Figure 3. Comparison of effective structure factors $S_{\rm eff}(q)$ of γB-crystallin solutions at 25 °C and at different concentrations with Baxter model calculations. Symbols are experimental data from SANS experiments; lines are calculated curves. (a) 46 mg ml^{-1}, (b) 92 mg ml^{-1}, (c) 179 mg ml^{-1} and (d) 255 mg ml^{-1}. (e) Effective structure factors $S_{\rm eff}(q)$ for γB-crystallin solutions plotted vertically as a function of q and protein concentration c, compared with the Baxter sticky sphere structure factor model with use of sphere diameter 3.6 nm and stickiness parameter $1/\tau = 8.62$ [39] (see text).

were not convoluted with the experimental resolution function of the SANS instrument, which additionally would smooth the sharp features of the dip and subsequent (local) maximum of $S_{\rm eff}(q)$. We note that the Baxter model has previously been successful at representing neutron scattering data on γB-crystallin solutions at lower concentrations, up to 86 mg ml^{-1} [26].

3.2. Proteins with short-range attraction and long-range repulsion—lysozyme

A completely different behaviour can be found for lysozyme at low ionic strength, where the long-range repulsive electrostatic potential due to the small number of charges present (approximately eight positive charges at pH = 7.8 [19, 36]) is only weakly screened and competes with the short-range attraction. In contrast, γB-crystallin has a net positive charge of 1.8 under our experimental conditions of pH 7.1 [40]. While short-ranged attraction dominates phase behaviour, structural and dynamic properties of concentrated lysozyme solutions at intermediate and high ionic strength, and leads to the well-known metastable liquid–liquid coexistence curve and a dynamically arrested gel or glass phase [16], critical phenomena in lysozyme are suppressed at low ionic strength, and we instead observe the formation of small equilibrium clusters over a large range of concentrations and temperatures [34]. This is illustrated in figure 4, where the scattered intensity $I(q)$ and the corresponding effective structure factor $S_{\rm eff}(q)$ obtained from SANS experiments with a concentrated lysozyme solution ($c = 248$ mg ml^{-1}) are shown as a function of temperature. A comparison with the corresponding data for the γB-crystallin solution at comparable concentration (figures 1(c), 2) immediately reveals the enormous differences. For the weakly screened solutions of the charged lysozyme the forward scattering is dramatically reduced, and a pronounced peak develops at a q value of $q_{\rm c}^* \approx 1$ nm^{-1}, with an additional shoulder at a higher q value of $q_{\rm m}^* \approx 2.5$ nm^{-1}.

The peak at $q_{\rm c}^*$ indicates strong positional correlations between the charged proteins, and it resembles at first sight the behaviour of colloidal particles at low ionic strength, where the strong long-range Coulomb repulsion leads to the formation of strongly correlated suspensions and colloidal crystals. Charged colloids at low ionic strength maximize their average interparticle distance d, and so d depends on the volume fraction ϕ and we find $q^* \approx 2\pi n^{1/3}$, where $n = 3\phi/(4\pi R^3)$ is the number density of particles with radius R. At the same time the forward scattering becomes suppressed upon increasing ϕ, owing to the decreased osmotic compressibility. However, a calculation of the effective structure factors $S_{\rm eff}(q)$ obtained by dividing $I(q)/c$ with the normalized intensity from a highly diluted lysozyme solution demonstrates obvious deviations from the situation encountered with charged colloid model systems. Figure 4(b) not only shows a measurable temperature dependence for the peak position $q_{\rm c}^*$, but also reveals a second peak at $q_{\rm m}^* \approx 2.5$ nm^{-1}, independent of temperature. On the basis of a detailed and quantitative analysis of systematic small-angle scattering experiments with concentrated lysozyme solutions, we were recently able to unambiguously demonstrate that under these conditions the proteins self-assemble into small clusters with a ϕ-dependent aggregation number $N_{\rm c}$ [34].

The driving force for such a self-assembly of lysozyme into small clusters comes from the short-range attraction between the proteins, which can be seen as an effective surface tension leading to a decrease in surface energy upon aggregation. On the other hand, cluster growth is limited by the increasing electrostatic energy of the clusters, which counterbalances the gain in surface energy and is due to the small number of residual charges combined with a low ionic strength. A low ionic strength ensures that the Debye length is larger or comparable to the cluster size. This balance between short-range attraction and weakly screened (and thus long-

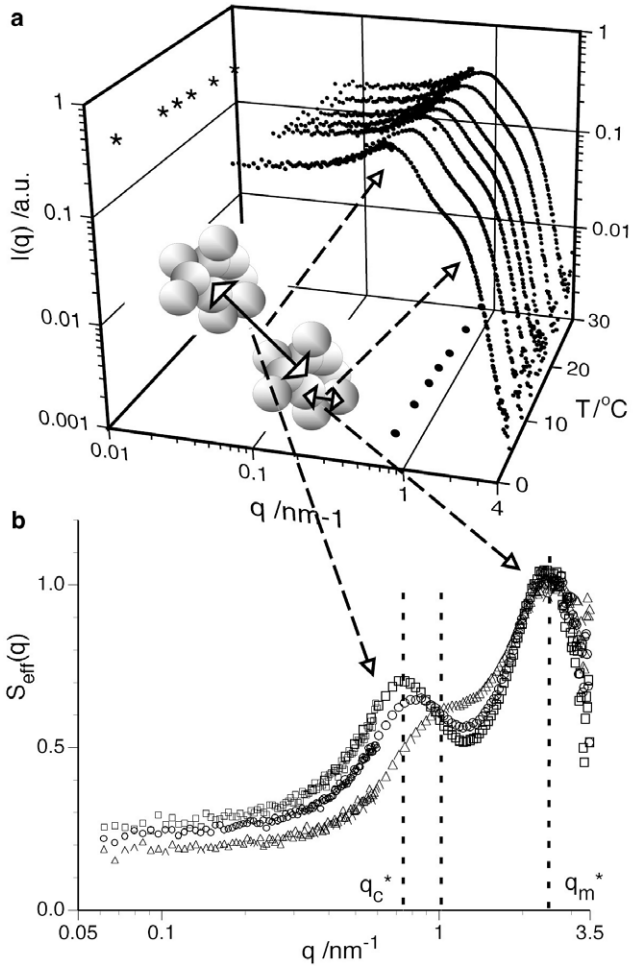

Figure 4. Scattered intensity $I(q)$ and corresponding effective structure factors $S_{\rm eff}(q)$ of a concentrated lysozyme solution as a function of temperature obtained by SANS. (a) $I(q)$ for a 248 mg ml^{-1} lysozyme in D_2O buffer at 5, 10, 14, 17, 20, 25 and 30 °C. Stars represent the $I(q)$ values extrapolated to $q = 0.01$ nm^{-1} and big filled circles show the projection of the peak maximum onto the q–T plane. (b) $S_{\rm eff}(q)$ for the sample in (a) at 5 (squares), 14 (circles) and 30 °C (triangles). The dashed lines highlight that decreasing the temperature shifts the cluster–cluster correlation peak $q_{\rm c}^*$ to lower q values, indicating fewer but larger aggregates while the monomer–monomer peak stays at a constant position $q_{\rm m}^*$.

range) electrostatic repulsion provides a stabilizing mechanism against gelation and determines a finite aggregation number $N_{\rm c}$, as in micelle formation. This cluster formation mechanism has in fact been seen in numerical simulations [13], and a corresponding theoretical model has been proposed for mesophase separation of colloids in organic solvents that has yielded an explicit expression for the concentration dependence of $N_{\rm c}$ [14].

This model allows us to assign the first peak in $S_{\rm eff}(q)$ at $q_{\rm c}^*$ (figure 4(b)) to cluster–cluster correlations caused by electrostatic interactions between the charged clusters, whereas the second peak at $q_{\rm m}^*$ reflects the positional correlations of the monomers within a single cluster. From our previous SANS and SAXS experiments we were able to demonstrate that the monomer peak at $q_{\rm m}^*$ exhibits a concentration and temperature independent value $q_{\rm m}^* R_{\rm m} \approx 3.8$,

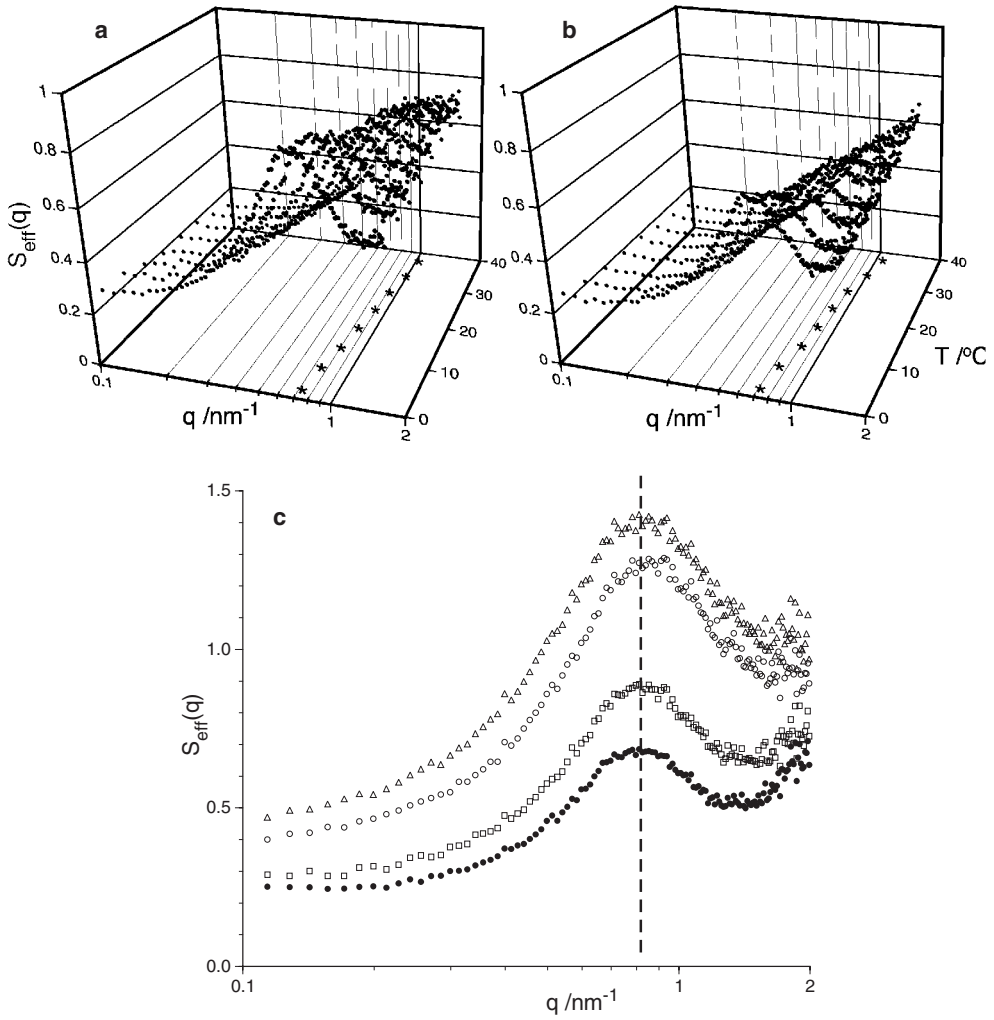

Figure 5. Effect of temperature on the effective structure factor $S_{\mathrm{eff}}(q)$ as obtained with SAXS. (a) 269 mg ml^{-1} and (b) 355 mg ml^{-1} lysozyme from 0 to 35 °C. Stars represent the position of the cluster–cluster correlation peak q_{c}^{*} projected onto the q–T plane. (c) $S_{\mathrm{eff}}(q)$ for lysozyme solutions at different concentrations c (82, 123, 269 and 355 mg ml^{-1} from top to bottom) at 5 °C. The cluster–cluster correlation peak q_{c}^{*} is constant for all c.

indicating a constant packing density within the cluster of approximately 60% by volume [34]. Moreover, we found that the position q_{c}^{*} of the cluster–cluster peak was also independent of ϕ at higher concentrations, which implies a constant cluster number density n_{c} (because $q_{\mathrm{c}}^{*} \propto n_{\mathrm{c}}^{1/3}$). This allows us to determine the dependence of N_{c} on ϕ according to $N_{\mathrm{c}} = n_{\mathrm{m}}/n_{\mathrm{c}} \propto \phi/n_{\mathrm{c}}$, where n_{m} is the monomer number density. Using a proportionality constant determined from a comparison with calculations using the Rogers–Young closure relation, we were subsequently able to determine N_{c} from q_{c}^{*} and ϕ as a function of protein concentration, and we were able to demonstrate that $N_{\mathrm{c}} \propto \phi$, in agreement with theoretical predictions [34].

In a next step we can now use the equilibrium cluster model in order to understand at least qualitatively the effect of temperature on the scattering data shown in figures 4 and 5.

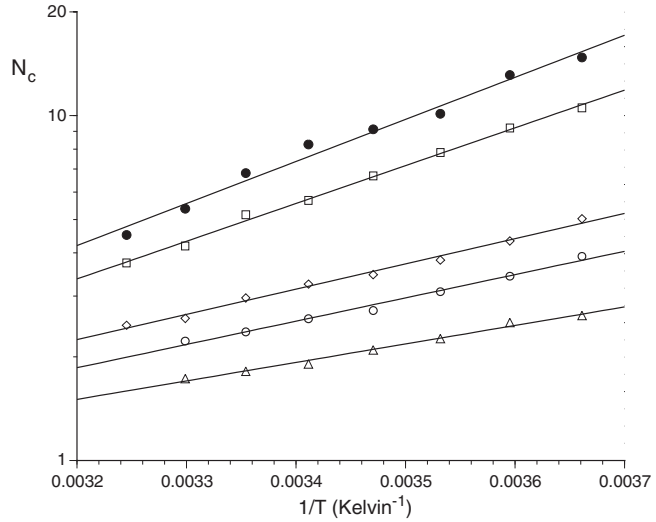

Figure 6. Arrhenius plot of the average cluster aggregation numbers N_c of lysozyme solutions as obtained from SAXS. The concentrations are 82, 123, 164, 269 and 355 mg ml^{-1} from bottom to top.

The forward intensity decreases only weakly with increasing temperature for all three protein concentrations (figure 4: 248 mg ml^{-1}, figure 5(a): 269 mg ml^{-1}, figure 5(b): 355 mg ml^{-1}), while the peak position q_c^* shifts from $q_c^* \approx 1$ nm^{-1} at 30 °C to $q_c^* \approx 0.75$ nm^{-1} at 5 °C, independent of concentration. The fact that q_c^* is concentration independent for a given temperature is further illustrated in figure 5(c), where $S_{\rm eff}(q)$ is shown for four different protein concentrations (82, 123, 269 and 355 mg ml^{-1}) at 5 °C. Our proposed scenario for equilibrium cluster formation governed by a subtle balance between opposing forces also provides the explanation for the effect of temperature: decreasing temperature favours attraction and leads to larger clusters and thus lower values of the cluster number density n_c, which subsequently shifts q_c^* to lower q values. It is important to point out that the effect of temperature is fully reversible, in full support of protein self-assembly into equilibrium clusters.

Figure 6 summarizes the effect of temperature on the cluster aggregation number N_c as obtained from a quantitative analysis of the peak position q_c^*. We see that N_c exhibits a pronounced concentration and temperature dependence and increases from values of $N_c \approx 2.2$ at $c = 123$ mg ml^{-1} and 30 °C to $N_c \approx 15$ at $c = 355$ mg ml^{-1} and 0 °C. Moreover, the temperature dependence follows a clear Arrhenius-like behaviour. It is interesting to note that a similar temperature dependence has been derived for micellar growth described by a multiple chemical equilibrium, once again indicating the similarity between the protein cluster formation and micelle formation. It is clear that we still lack a detailed thermodynamic model for our system that would allow us to extract the underlying cluster energy as a function of concentration and temperature, but we are currently working on a corresponding analysis of our data.

Acknowledgments

We thank Frederic Cardinaux for his help in sample preparation and the Swiss spallation neutron source SINQ, Paul Scherrer Institute, Villigen, Switzerland, for the neutron beam time. We

gratefully acknowledge the expert help of our local contacts at PSI, Joachim Kohlbrecher and Steven van Petegem. We are deeply grateful for precious and fruitful discussions with Stefan Egelhaaf and Willem Kegel. This work was supported by the Swiss National Science Foundation, the Marie Curie Network on Dynamical Arrest of Soft Matter and Colloids (MRTN-CT-2003-504712), and the National Institutes of Health, USA (NIH EY 11840, GT).

References

[1] Dawson K A 2002 *Curr. Opin. Colloid Interface Sci.* **7** 218
[2] Trappe V, Prasad V, Cipelletti L, Segré P N and Weitz D A 2001 *Nature* **411** 772
[3] Sciortino F 2002 *Nat. Mater.* **1** 145
[4] Pham K N *et al* 2002 *Science* **296** 104
[5] Eckert T and Bartsch E 2002 *Phys. Rev. Lett.* **89** 125701
[6] Weeks E R, Crocker J C, Levitt A C, Schofield A and Weitz D A 2000 *Science* **287** 627
[7] Foffi G *et al* 2002 *Phys. Rev.* E **65** 031407
[8] Bergenholtz J, Poon W C K and Fuchs M 2003 *Langmuir* **19** 4493
[9] Yethiraj A and van Blaaderen A 2003 *Nature* **421** 513
[10] Poon W C K 2002 *J. Phys.: Condens. Matter* **14** R859
[11] Pham K N, Egelhaaf S U, Pusey P N and Poon W C K 2004 *Phys. Rev.* E **69** 11503
[12] Puertas A M, Fuchs M and Cates M E 2004 *J. Chem. Phys.* **121** 2813
[13] Sciortino F, Mossa S, Zaccarelli E and Tartaglia P 2004 *Phys. Rev. Lett.* **93** 055701
[14] Groenewold J and Kegel W K 2001 *J. Phys. Chem.* B **105** 11702
[15] Segré P N, Prasad V, Schofield A B and Weitz D A 2001 *Phys. Rev. Lett.* **86** 6042
[16] Kulkarni A M, Dixit N M and Zukoski C F 2003 *Faraday Discuss.* **123** 37
[17] Muschol M and Rosenberger F 1997 *J. Chem. Phys.* **107** 1953
[18] Malfois M, Bonneté F, Belloni L and Tardieu A 1996 *J. Chem. Phys.* **105** 3290
[19] Broide M L, Tomic T M and Saxowsky M D 1996 *Phys. Rev.* E **53** 6325
[20] Schurtenberger P, Chamberlin R A, Thurston G M, Thomson J A and Benedek G B 1989 *Phys. Rev. Lett.* **63** 2064
Schurtenberger P, Chamberlin R A, Thurston G M, Thomson J A and Benedek G B 1993 *Phys. Rev. Lett.* **71** 3395 (erratum)
[21] Benedek G B, Pande J, Thurston G M and Clark J I 1999 *Prog. Retinal Eye Res.* **18** 391
[22] Thomson J A, Schurtenberger P, Thurston G M and Benedek G B 1987 *Proc. Natl Acad. Sci. USA* **84** 7079
[23] Broide M L, Berland C R, Pande J, Ogun O and Benedek G B 1991 *Proc. Natl Acad. Sci. USA* **88** 5660
[24] Berland C R, Thurston G M, Kondo M, Broide M L, Pande J, Ogun O and Benedek G B 1992 *Proc. Natl Acad. Sci. USA* **89** 1214
[25] Liu C-W, Lomakin A, Thurston G M, Hayden D L, Pande A, Pande J, Ogun O, Asherie N and Benedek G B 1995 *J. Phys. Chem.* **99** 451
[26] Petitt P, Edwards M E and Forciniti D 1997 *Eur. J. Biochem.* **243** 415
[27] Bonneté F, Malfois M, Finet S, Tardieu A, Lafont S and Veesler S 1997 *Acta Crystallogr.* D **53** 438
[28] Koretz J F, Cook C A and Kaufman P L 1997 *Invest. Ophthalmol. Vis. Sci.* **38** 569
[29] Lomakin A, Asherie N and Benedek G B 1996 *J. Chem. Phys.* **104** 1646
[30] Asherie A, Lomakin A and Benedek G B 1996 *Phys. Rev. Lett.* **77** 4832
[31] Lomakin A, Asherie N and Benedek G B 1999 *Proc. Natl Acad. Sci. USA* **9** 9465
[32] Piazza R 2000 *Curr. Opin. Colloid Interface Sci.* **5** 38
[33] Benedek G B 1997 *Invest. Ophthalmol. Vis. Sci.* **38** 1911
[34] Stradner A, Sedgwick H, Cardinaux F, Poon W C K, Egelhaaf S U and Schurtenberger P 2004 *Nature* **432** 492
[35] Thurston G M, Pande J, Ogun O and Benedek G B 1999 *Invest. Ophthalmol. Vis. Sci.* **40** 299
[36] Tanford C and Roxby R 1972 *Biochemistry* **11** 2192
[37] Stradner A, Thurston G, Lobaskin V and Schurtenberger P 2004 *Prog. Colloid Polym. Sci.* **126** 173
[38] Fine B M, Pande J, Lomakin A, Ogun O O and Benedek G B 1995 *Phys. Rev. Lett.* **74** 198
[39] Fine B M, Lomakin A, Ogun O O and Benedek G B 1996 *J. Chem. Phys.* **104** 326
[40] Shand-Kovach I 1986 *PhD Thesis* MIT